Applied Catalysis B: Environmental 89 (2009) 128–136

Contents lists available at ScienceDirect

Applied Catalysis B: Environmental

journal homepage: www.elsevier.com/locate/apcatb

CO oxidation on Au nanoparticles supported on wormhole HMS material: Effect of support modification with CeO_2

José A. Hernandez [a], S. Gómez [a], B. Pawelec [b], T.A. Zepeda [c,*]

[a] Área de Ingeniería Química, Universidad Autónoma Metropolitana-Iztapalapa, Iztapalapa 09340, D.F., Mexico
[b] Instituto de Catálisis y Petroleoquímica, CSIC, c/Marie Curie 2, Cantoblanco, 28049 Madrid, Spain
[c] Centro de Nanociencias y Nanotecnología – Universidad Nacional Autónoma de México, Km. 107 Carretera Tijuana-Ensenada, 22800 Ensenada, B.C. Mexico

ARTICLE INFO

Article history:
Received 1 August 2008
Received in revised form 30 November 2008
Accepted 6 December 2008
Available online 13 December 2008

Keywords:
HMS
Cerium
Supported Au catalyst
CO oxidation
Support effect
Physical characterization

ABSTRACT

This paper describes the performance of Au catalysts supported on wormhole hexagonal mesoporous silica (HMS) for the CO oxidation reaction, and the effect of support modification with cerium on the catalysts for this reaction. Supports and catalysts were characterized by N_2 adsorption–desorption, XRD, HRTEM, DRS UV–vis, TPR and XPS. The HMS material was prepared by the surfactant neutral S^0I^0 templating route, and its modification with cerium was performed by direct synthesis (Ce-HMS) and impregnation (Ce/HMS) methods. Gold was deposited via the deposition–precipitation method. After calcination at 573 K for 3 h, the Au nanoparticles with sizes in the range 3.8–4.9 nm were formed. The smallest Au particles were formed on the Ce/HMS support with small crystals of CeO_2 phase on its surface, as shown by XRD. In general, Ce-containing Au catalysts were found to be more active in CO oxidation than the Ce-free Au/HMS counterpart, with the direct synthesis method of the cerium incorporation being less effective than the impregnation method. The highest activity of the Au/Ce-HMS catalyst in CO oxidation was associated with its higher gold dispersion and larger degree of coverage of HMS by CeO_2, thereby increasing the effectiveness of oxygen mobility.

1. Introduction

The high increase in the use of automobiles for transportation has led to a rising demand for fossil fuels. Consequently, and also due to the incomplete combustion of fuels in both Otto and Diesel engines, the amount of pollutant gases, such as CO, NO and several hydrocarbons, has increased considerably in recent years [1]. To comply with emission standards, automotive exhausts have to be treated with catalytic converters that oxidize CO and hydrocarbons to CO_2 and also reduce NO to N_2 [1–3].

Although gold was long regarded as chemically inert because of its completely filled d-band [4], this situation changed when Haruta with co-workers showed that CO oxidation could be archived at a low temperature if very small gold nanoparticles were formed on suitable supports [5–7]. This is because one of the factors that might have a bearing on the gold particle sizes is their interaction with support [4]. Apart from the moderate metal-support interaction (MSI), the use of transition metal oxides as supports was proven to increase oxygen mobility in the oxidation reaction and induce electronic effects, improving thermal stability or decreasing the sintering of Au particles [8]. The influence of the catalyst preparation method, type of support, pre-treatment conditions and Au particle size on the catalytic response of gold catalysts in CO oxidation was extensively reviewed by Bond and Thomson [4]. In particular, Au catalysts supported on Fe_2O_3 or TiO_2 materials were found to be promising for CO oxidation at temperatures below 273 K [5,6]. It has recently been reported that the gold clusters (not the complexes) on high-area cerium oxide are highly active in CO oxidation [9].

Recently, both MCM-41 and SBA-15 materials have attracted attention as new potential supports for the preparation of supported Au catalysts that are highly active in the CO oxidation reaction [10–13]. In particular, an attempt was made to disperse Au nanoparticles directly inside the mesoporous MCM-41 matrix [14]. However, the catalytic activity of the Au/MCM-41 sample for CO oxidation was not high enough due to the inertness of the silica support and the internal blockage of long 1D channels of MCM-41 by Au nanoparticles [14]. Some enhancement of activity in the CO oxidation on the Au/MCM-41 catalysts was recorded when the catalyst was prepared by a one-pot synthesis method, in which the quaternary ammonium salt C_{16}TMAB (surfactant) acts as protecting agent for Au nanoparticles and as a mesostructural template [15]. Compared to straight pores in MCM-41, a two-dimensional hexagonal structure of aerosol-derived silica was found to be much better as a support because it can trap nanoparticles and restrict the mobility of species that lead to thermal sintering [16].

* Corresponding author. Tel.: +52 6461744602x353; fax: +52 6461744603.
E-mail address: trino@icp.csic.es (T.A. Zepeda).

0926-3373/$ – see front matter © 2008 Elsevier B.V. All rights reserved.
doi:10.1016/j.apcatb.2008.12.005

Similarly, Overbury et al. [17] observed that Au nanoparticles located within wormhole silica yield lower particle size after reduction at 773 K. The other way to avoid Au particle sintering is through support modification with transition metal oxides. In this sense, it was shown that the presence of transition metal oxides in the MCM-41 material decreases the size of gold particles during calcination [18]. Although hexagonal mesoporous silica (HMS) has similar textural properties to MCM-41 and SBA-15 materials (a large specific area, a hexagonal array and uniform pore channels), these two materials (MCM-41 and SBA-15) have no high hydrophobicity property in comparison with the HMS material. It is very well-known that the matter type HMS exhibits high hydrophobicity ability, this property could have an advantage about the hydrothermal stability for the presence of water formed during the reaction of the CO oxidation. Additionally, the application of HMS as support for the preparation of supported Au catalysts for the CO oxidation has not yet been studied. Moreover, to the best of our knowledge, CO oxidation on Au catalysts supported on HMS modified with CeO_2 has not been reported in the literature.

Within this scenario, the present work investigates the potential use of novel mesoporous Ce-containing HMS materials as supports for the preparation of Au catalysts via the deposition–precipitation method. The HMS material was prepared by the surfactant neutral S^0I^0 templating route and the effect of the method of cerium introduction (direct synthesis versus impregnation methods) was studied. Pure supports and Au catalysts (in their calcined and spent forms) were characterized by N_2 adsorption–desorption, XRD, DRS UV–vis, TPR and XPS. The catalytic activities of supported Au catalysts were evaluated in the CO oxidation reaction performed in a flow reactor at atmospheric pressure and in the 293–673 K temperature range.

2. Experimental

2.1. Synthesis of the HMS, Ce-HMS and Ce/HMS supports

Wormhole hexagonal mesoporous silica (HMS) material was synthesized by the neutral S^0I^0 templating route as described previously [19], which is based on hydrogen bonding and self-assembly between neutral primary amine surfactants (S^0) and a neutral inorganic precursor (I^0). Dodecylamine (Aldrich 99 %) was employed as surfactant, and mesitylene (C_9H_{12}, Aldrich 98%) was added to the reaction mixture as the swelling organic agent, as first proposed by Kresge et al. [20]. The Ce-modified HMS material (Ce-HMS) was prepared by a similar method to HMS synthesis, but Ce was incorporated during direct synthesis using cerium nitrate hexahydrate (Aldrich 99%) as Ce precursors. The Ce-HMS material was synthesized with a Si/Ce atomic ratio equal to 40. The reaction products were filtered, washed with distilled water and dried at room temperature for 48 h, followed by drying at 328 K for 4 h, and then the samples were calcined at 800 K for 4 h in static air, with a heating rate of 4 K min^{-1}.

The Ce-supported material (Ce/HMS) was prepared by impregnation of the HMS support using the pore filling method. The pure HMS material was impregnated with 1.5 cm^3 g^{-1} of an aqueous solution of cerium nitrate hexahydrate (Aldrich 99%), whose concentration was selected to obtain 6.9 wt% Ce. The impregnated samples were dried and calcined under the same conditions described previously.

2.2. Catalyst preparation

The supported Au catalysts were prepared via the deposition–precipitation method using the $HAuCl_4$ as gold precursor. A solution of chloroauric acid in water was slowly added to a stirred suspension of 2 g of support in water. The pH of the solution was kept close to 10, with aqueous ammonia (Merck, 25%), and the solution was aged for 30 min at room temperature. The catalyst was washed repeatedly with distilled water, dried in air overnight at 323 K, and then calcined at 573 K for 3 h in static air atmosphere. The chemical composition of pure supports and oxide Au catalysts are shown in Table 1.

Table 1
Chemical composition of pure supports and oxide Au catalysts.

Sample	Au (wt%)[a]	CeO_2 (wt%)[a]
HMS	–	–
Ce-HMS	–	6.7
Ce/HMS	–	6.9
Au/HMS	0.59	–
Au/Ce-HMS[b]	0.65	6.6
Au/Ce/HMS[c]	0.67	6.8

[a] Au and CeO_2 wt% was derived from chemical analysis (ICP).
[b] Cerium incorporated into HMS by direct synthesis method.
[c] Cerium incorporated into HMS by impregnation method.

2.3. Characterization methods

2.3.1. N_2 adsorption–desorption isotherms

The nitrogen adsorption–desorption isotherms of the pure supports and spent (sample after CO oxidation) Au catalysts were determined on an ASAP 2000 Micromeritics device. Prior to the experiments, the samples were degassed at 543 K in a vacuum for 5 h. The volume of adsorbed N_2 was normalized to standard temperature and pressure. Specific surface area (S_{BET}) was calculated by the BET equation applied to the range of relative pressures $0.05 < P/P^0 < 0.30$. The average pore diameter was calculated by applying the Barret–Joyner–Halenda method (BJH) to the desorption branches of the N_2 isotherms. The cumulative pore volume was obtained from the isotherms at $P/P^0 = 0.99$. The volume was obtained at relative pressure $P/P^0 = 0.99$.

2.3.2. X-ray diffraction

The low-angle and high-angle X-ray patterns of spent Au catalysts in the 2θ range at a step of 0.02° were recorded on a Rigaku 2100 diffractometer, using a monochromatic Cu Kα radiation ($\lambda = 0.1541$ nm) and a glass support.

2.3.3. High resolution transmission electron microscopy (HRTEM)

HRTEM studies were carried out using a JEM 2100F microscope operating with a 200 kV accelerating voltage. Spent Au catalysts were ground into a fine powder and dispersed ultrasonically in hexane at room temperature. A drop of the suspension was then put on a carbon-coated Cu grid. At least 10 representative images were taken for each sample. In order to obtain statistically reliable information, the length of ca. 200 particles was measured. Particle size distributions were obtained by counting more than ca. 200 particles for each sample. Particle size diameters were calculated with the equation $d_{avg} = \Sigma(n_i d_i)/\Sigma n_i$.

2.3.4. UV–vis diffuse reflectance spectroscopy

UV–vis diffuse reflectance spectra (DRS UV–vis) of the pure supports and spent Au catalysts were recorded using a Cary 5_E spectrophotometer with a specially designed Praying Mantis diffuse reflection cell (Harrick) for in situ measurements. All spectra were recorded after heating the samples at 523 K in He flow for 1 h. The spectrum of the corresponding support was subtracted from the spectrum of the catalyst. The decomposition of each spectrum was performed by non-linear fitting of multiple Gaussian peak functions sharing a common baseline.

2.3.5. Temperature-programmed reduction (TPR)

TPR experiments of the freshly calcined catalysts were carried out in a semiautomatic Micromeritics TPD/TPR 2900 apparatus interfaced to a microcomputer. TPR profiles were obtained by passing a 10% H_2/Ar flow (50 mL/min) through the sample. The temperature was increased at a rate of 10 K/min, and the amount of H_2 consumed was determined with a thermoconductivity detector (TCD). The effluent gas was passed through a cold trap before the TCD in order to remove water from the exit stream.

2.3.6. X-ray photoelectron spectroscopy (XPS)

X-ray photoelectron spectra of freshly calcined and spent Au catalysts were recorded in order to study the effect of HMS material modification with Ce on the dispersion and oxidation state of supported gold species. A VG Escalab 200R spectrometer equipped with a hemispherical electron analyzer and a Mg Kα ($h\nu$ = 1253.6 eV) X-ray source was used. Samples were first placed in a copper holder mounted on a sample-rod in the pre-treatment chamber of the spectrometer and then outgassed at 403 K for 1 h before transfer to the analysis chamber. All samples were outgassed at 10^{-5} mbar and then transferred to the ion-pumped analysis chamber, where residual pressure was kept below 7×10^{-9} mbar during data acquisition. The binding energies (BE) were referenced to the C 1s peak (284.9 eV) to account for the charging effects. The areas of the peaks were computed after fitting the experimental spectra to Gaussian/Lorentzian curves and removal of the background (Shirley function). Surface atomic ratios were calculated from the peak area ratios normalized by the corresponding atomic sensitivity factors.

2.3.7. Catalytic activity measurements

CO oxidation was carried out in a bed quartz micro-reactor connected on-line to a GC Shimadzu 12-A (5-A and Porapack Q) with two packed column; equipped with a TCD. 300 mg of the freshly calcined sample was introduced into the micro-reactor, and the sample was then contacted with a gas mixture (1, 0.5, 0.33 and 98.17 % v/v of CO, O_2, H_2 and N_2, respectively, 100 mL/min of total flow). The activities of gold catalysts were evaluated at atmospheric pressure and working in a 293–673 K temperature range with a heating rate of 3 K min^{-1}.

3. Results and discussion

3.1. N_2 adsorption–desorption isotherms

The nitrogen adsorption isotherms of the pure supports and spent gold catalysts tested in the CO reaction are shown in Fig. 1. The isotherms of all samples are type IV, according to the IUPAC classification [21], with a sharp step at intermediate relative pressures. All samples have two capillary condensation steps: (i) the first hysteresis loop for these materials starts at a partial pressure of about 0.30–0.45, indicating the presence of framework mesoporosity and (ii) the second hysteresis loop starting at a partial pressure of about 0.80–0.85 is due to textural inter-particle mesoporosity or macroporosity. The sharp inflection of the adsorption branch confirms the high quality of materials with uniform mesoporosity. The appreciable type H1 hysteresis loops indicate the presence of textural and cylindrical mesopores [22].

The specific area (S_{BET}), average pore volume (V_p) and average pore diameter of pure supports and used gold catalysts are listed in Table 2. The Ce-free support shows the higher specific area value in comparison with the Ce-content samples (Ce-HMS and Ce/HMS). The Ce-HMS material recorded both higher average pore diameter value (5.2 nm) and pore volume (1.65 $cm^3\ g^{-1}$) in comparison with the other two samples. Considering the study by Gac et al. [18], the mechanism of template removal during calcination of the Ce-HMS material prepared by direct synthesis method could be different to those in the case of Ce/HMS material prepared by impregnation of the calcined HMS. In the former case, the formation of a more rigid structure with slightly smaller pores could be expected [18]. However, our N_2 adsorption–desorption data did not indicate major differences in the textural properties of the pure supports studied.

A comparison of the specific surface area values of the pure supports and calcined catalysts indicates that S_{BET} lightly decreased upon the incorporation of gold (Table 2). Since the spent catalysts show only a slightly lower S_{BET} than their calcined counterparts (the changes are within the experimental error), pore blockage due to large gold particles formed from the gold phase sintering can be excluded. The highest specific area value is observed in the spent Au/Ce/HMS sample. Average pore volume also decreases both after gold species incorporation during catalyst

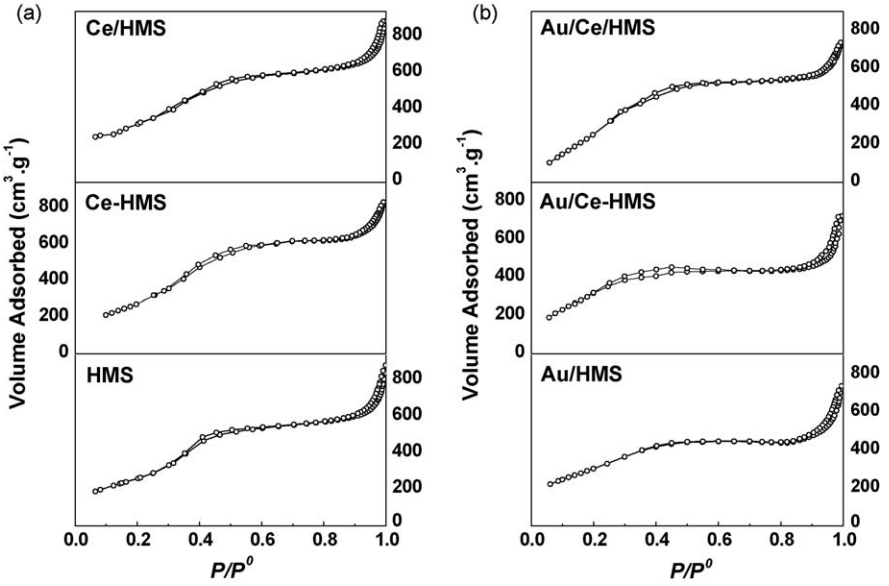

Fig. 1. Nitrogen adsorption–desorption isotherms of pure supports (a) and spent Au catalysts (b).

Table 2
Textural properties of the support, calcined and spent Au catalysts in the CO oxidation.

Sample	S_{BET} ($m^2\ g^{-1}$)		Pore diameter (nm)		Pore volume ($cm^3\ g^{-1}$)		NS_{BET}[a]		d_{100} (nm)[b]		a_0 (nm)[c]	Wall thickness (nm)[d]
HMS	770		5.1		1.32		1		8.48		9.8	4.7
Ce-HMS	743		5.2		1.65		1		8.54		9.9	4.7
Ce/HMS	763		5.1		1.61		1		8.54		9.9	4.8
	Cal.	Used	Cal.	Used	Cal.	Used	Cal.	Used				
Au/HMS	711	702	5.1	5.1	1.28	1.27	0.93	0.92	8.48		9.8	4.7
Au/Ce-HMS	734	726	5.2	5.2	1.61	1.60	0.99	0.98	8.53		9.8	4.6
Au/Ce/HMS	760	751	5.1	5.1	1.65	1.63	1	0.99	8.53		9.8	4.7

[a] NS_{BET}: normalized S_{BET} as calculated from equation $NS_{BET} = (S_{BET\ of\ catalyst})/[(1-y) \times S_{BET\ of\ support}]$; y is the weight fraction of the phases.
[b] d-Spacing is calculated from the X-ray patterns of the spent samples.
[c] Unit cell parameter a_0 is calculated by $(2d_{100})/(\sqrt{3})$.
[d] Wall thickness is obtained by subtracting pore size from the unit cell parameter.

preparation and after the on-stream reaction of CO oxidation over freshly calcined catalysts. The highest pore volume value is observed in the spent Au/Ce/HMS catalysts. The average pore diameter of the oxide gold catalysts remains virtually the same as the values observed in the pure supports. We could therefore conclude that the structural parameters are preserved after reaction. Table 2 shows the values of normalized specific surface area (NS_{BET}) of calcined and spent catalysts. The NS_{BET} values are close to 1 for both Ce-containing catalysts, while those of the Au/HMS sample are ca. 0.93. This might indicate that the specific morphology of both Ce-containing supports favours the location of the gold particles on the support surface. It is noteworthy that, irrespectively of the method of HMS modification by Ce, there is no difference between the NS_{BET} of the calcined and spent catalysts, suggesting the high stability of gold particles during on-stream reaction.

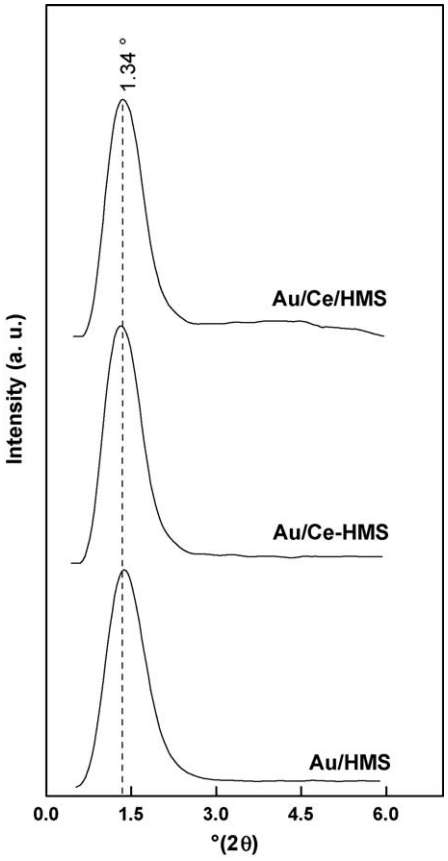

Fig. 2. XRD studies of spent Au catalysts at low angles.

3.2. Low- and wide-angle X-ray diffraction

The low-angle X-ray diffractograms of the spent gold catalysts are shown in Fig. 2. All samples show an intense reflection at 1.34°. This peak is characteristic of wormhole structures, assembled from neutral, long alkyl chain amines, which possess short range hexagonal symmetry with uniform pore diameter [23–25]. One can note that, irrespectively of the presence of Ce ions, all XRD peaks are virtually similar, indicating that no important changes in the wormhole structure of support occur during on-stream conditions, in good agreement with the N_2 adsorption–desorption results. This conclusion is also supported by the value of the wall thickness parameter, which changes insignificantly after the deposition of the gold onto the surface of the supports.

Fig. 3 shows the XRD patterns of the spent gold catalysts recorded in the 10–60° range in 2θ intervals. A broad band is observed between 15° and 35°, corresponding to the amorphous part of the supports. No reflections belonging to gold and cerium oxides were observed. The absence of the gold and cerium (in the correspond case) diffractions in the catalyst could indicate that there are no segregate Au or Ce phase on the surface and/or the presence of Au and Ce particles are non-crystalline or are well-dispersed with a particle size lower than 5 nm (according to the detection sensitivity of the diffractometer). Then we could conclude that the deposition of Au phase on the HMS (with or without cerium content) resulting in the formation of supported Au particles well-dispersed.

3.3. High-resolution transmission electronic microscopy

The HRTEM study was carried out in order to compare the average Au particle size of the spent catalysts tested in the CO

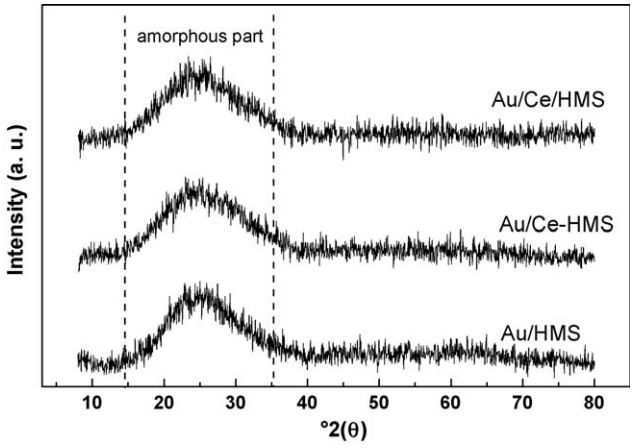

Fig. 3. XRD studies of spent Au catalysts at wide angles.

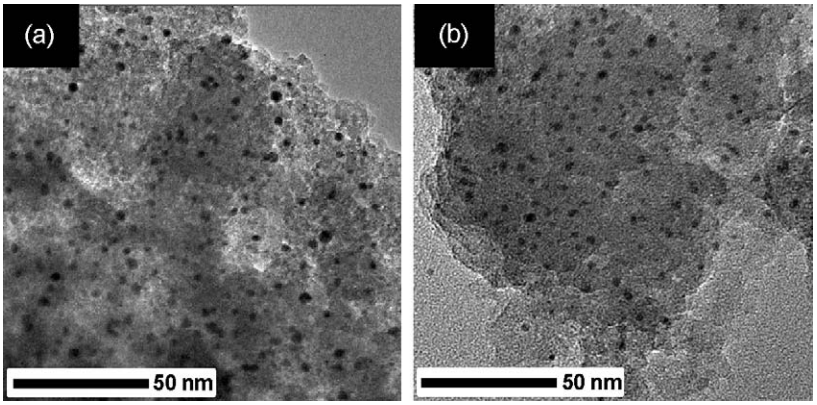

Fig. 4. HRTEM image of freshly reduced (a) and spent Au/Ce/HMS catalyst (b).

oxidation at 673 K. For example, Fig. 4(a) and (b) shows the HRTEM image of the freshly reduced and spent Au/Ce/HMS catalyst, respectively. Similarly to this catalyst, the others two samples (Au/HMS and Au/Ce-HMS catalysts) have a homogeneous distribution of Au particles. The HRTEM average Au size particles were 4.9, 4.2 and 3.6 nm for Au/HMS, Au/Ce-HMS and Au/Ce/HMS catalysts, respectively. We might therefore assume that the HMS support modification with Ce favours the formation of smaller gold particles on the support surface. It is noteworthy that the presence of CeO_2 species located on the HMS surface (Ce/HMS) is more favourable for gold particle dispersion than the incorporation of Ce ions into the HMS framework by the direct synthesis method. Finally, analysing the HRTEM images showed in Fig. 4(a) and (b), we can note that are not significant changes in the morphologic and size (by sintering process) of supported Au particles during on-stream conditions occurs. This observation also is valid for the others two samples and these observations are in agreement with the S_{BET} results.

3.4. UV–vis diffuse reflectance spectroscopy

It is known that ceria is a semiconductor with band gap energy (E_g) of 2.94 eV. Thus, it could be activated by irradiation with light in the near UV–vis range [26]. DRS has also been used extensively to study ceria-based materials and transition metal oxides to obtain information on surface coordination and on the different oxidation states of metal ions by measuring their d–d and f–d transitions and the oxygen–metal ion charge transfer bands. However, this technique has limitations due to the difficulty in interpreting large band widths and the specular reflectance often observed in Ce spectra [27].

We have investigated the coordination of Ce ions in supports and the effect of the presence of Ce ions on the electronic Au structure. Fig. 5 shows the electronic spectra of supports and used Au catalysts. For comparative purposes, Fig. 5(a) includes the electronic spectrum of the pure CeO_2 oxide. This oxide showed two intense absorption bands. The band at 248 nm can be attributed to the electronic transition with charge transfer ($O_2^- \rightarrow Ce^{4+}$) associated to Ce ions in SiO_2 [28], while the latter (489 nm) can be assigned to the inter-band transitions taking place in Ce_2O_3 that could be associated to the presence of Ce ions in octahedral coordination. As expected, the electronic spectrum of the HMS support did not show any electronic transition (Fig. 5(a)). By contrast, all Ce-content samples showed an intense absorption band around 248 nm, which is due to electronic transition ligand-to-metal with a charge transfer (LMCT) associated with Ce^{4+} ions in tetrahedral coordination. An additional absorption band around 489 nm was observed in the supported Ce sample (Ce/HMS) and this could be attributed to the presence of octahedral Ce ions. We note that practically all Ce-ions in the Ce-HMS spectrum are

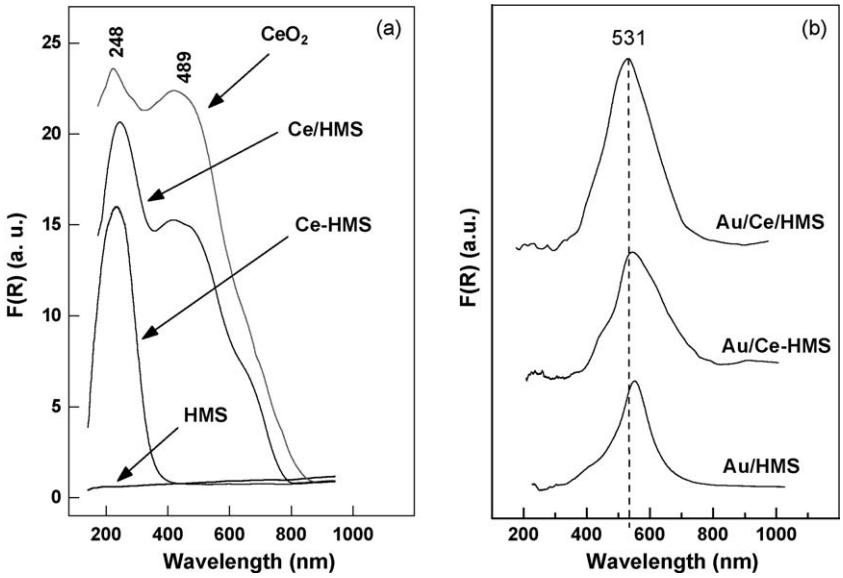

Fig. 5. DRS UV–vis spectra of pure supports (a) and spent Au catalysts (b).

incorporated into the HMS structure. Nevertheless, the band intensity corresponding to tetrahedral Ce ions is more intense in the supported Ce sample. In addition, this sample recorded a highly intense signal associated with octahedral Ce ions. This could be attributed to higher surface Ce concentration in the supported Ce sample. This sample is very interesting and one could expect a different behaviour in catalytic activity.

After the subtraction from the UV–vis spectra of their homologous support, all DRS UV–vis spectra of used gold catalysts have an intense band at 531 nm (Fig. 5(b)). This band is attributed to the surface plasmon resonance of gold nanoparticles [29]. The presence of plasmon band arises from the collective oscillations of the free conduction band electrons that are induced by incident electromagnetic radiation when the wavelength of the incident light greatly exceeds particle diameter [30]. We note that the intensity of this band is very low and its position depends on Au particle size and shape, and in our case it seems that it also depends on the presence of Ce. We could note that the Au/HMS sample showed the lower intensity of the Au surface plasmon resonance (SPR) and this band is centred at higher wavelength, in comparison with the others Ce-content samples. These observations could be associated with multiplex effects such as particle size, shape, interparticle distance (due to their mutual dipole–dipole interaction) and the local refraction index. Contrary to this sample, the higher intensity, the lower the wavelength and the higher the width of the plasmon signal observed in the supported Ce sample (Au/Ce/HMS). This could be related to the presence of a higher amount of metallic Au particles of lower size, as indicated by the XRD and HRTEM results. With these results, we can conclude that higher amounts of Au^0 nanoparticles are formed during reaction when Ce ions are supported on the HMS surface and not when the Ce ions are incorporated into the HMS framework.

3.5. Temperature-programmed reduction

Fig. 6 shows the TPR profiles of freshly calcined gold catalysts after the subtraction of their homologous support TPR profile. They all showed an intense reduction peak around 420–460 K. An additional shoulder around 619 K was observed in Ce-containing samples. The low temperature reduction peak around 420–460 K is related to the reduction of oxidized $Au^{3+} \rightarrow Au^{1+}$ ($Au_2O_3 + 2H_2 \rightarrow Au_2O + 2H_2O$); the reduction peak observed at 619 K is associated with the reduction of $Au^{1+} \rightarrow Au^0$ ($Au_2O + H_2 \rightarrow Au^0 + H_2O$) [31,32]. The lower reduction temperature of the first gold reduction ($Au^{3+} \rightarrow Au^{1+}$) was observed in the Au/Ce-HMS sample (420 K), while this peak in the Au/Ce/HMS and Au/HMS samples is observed toward higher temperature (around 446 and 462 K, respectively). We also note that hydrogen consumption is higher in Ce-content catalysts in comparison with the Ce-free sample, but higher H_2 consumption is observed in the supported Ce-catalyst (Au/Ce/HMS). This observation could be associated with (i) a higher dispersion and (ii) lower interaction of Au species on the Ce/HMS support, in comparison with the others samples. The presence of Ce ions in gold catalysts has an important effect on the reducibility and dispersion of the gold phase. Significantly, the amount of consumed H_2 corresponding to the reduction of Au^{1+} species in Au^0 is higher in the Au/Ce/HMS sample, in comparison with the other samples (Fig. 6). This could indicate that the presence of Ce ions on the HMS surface had a strong impact on the formation and stability of supported metallic gold particles.

3.6. X-ray photoelectron spectroscopy (XPS)

The XPS technique was used to determine the effect of HMS support modification with cerium on the chemical state of gold species and their surface exposure after precursor calcination at

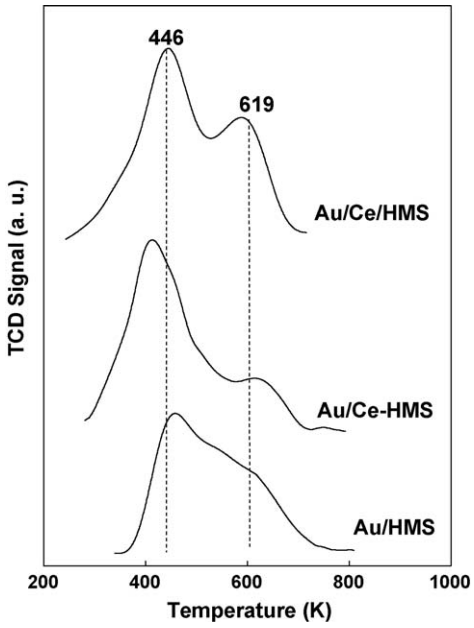

Fig. 6. TPR profiles of calcined Au catalysts supported on HMS, Ce-HMS and Ce/HMS materials.

573 K and their use in CO oxidation at 673 K. Fig. 7(a) and (b) shows the XPS spectra of the Au 4f core electron level for freshly calcined and spent catalysts, respectively. The binding energy values of the peak of gold (Au $4f_{7/2}$), surface Au/Si atomic ratio and $Au^0/(Au^0 + Au^{3+})$ ratio are listed in Table 3. All freshly calcined gold catalysts have a principal Au $4f_{7/2}$ peak around 85.6 ± 0.1 eV indicating the presence of Au^{3+} species associated with Au_2O_3 phase [33,34]. As seen in Fig. 7(a), the Au/Ce/HMS catalyst records an Au $4f_{7/2}$ signal that is more intense and wider than in the other two catalysts. This is because this sample has an additional Au $4f_{7/2}$ peak at 84.1 eV, which is associated with the presence of metallic gold particles [35,36]. The high $Au^0/(Au^0 + Au^{3+})$ ratio (0.19) of this catalyst indicates the easier reduction of its gold oxide species, in good agreement with the TPR results (*vide supra*). By analyzing the Au/Si atomic ratios of the freshly calcined samples (Table 3), one might note that the cerium-free Au/HMS sample shows lower Au species surface exposure than both Ce-containing counterparts. The amount of Au species on the surface of all catalysts follows the order: Au/Ce/HMS > Au/Ce-HMS > Au/HMS. In comparison with the Au/Ce-HMS and Au/HMS samples, the calcined Au/Ce/HMS catalyst has 20% and 75% higher surface exposure of gold species, respectively. Thus, the method of incorporating Ce ions onto the HMS material had a major effect on the surface exposure and oxidation state of gold species. Considering the XPS data (*vide supra*), one might conclude that the presence of CeO_2 on the HMS support surface enhanced Au species surface exposure and their reduction.

Considering the chemical state of Au species in the spent catalysts, one might note that all catalysts show one intense Au $4f_{7/2}$ signal at 84.4 eV, characteristic of the presence of Au^0 species (Fig. 7(b)). Additionally, the Au/HMS and Au/Ce-HMS samples exhibit one low intensity signal at 85.5 eV, which could be ascribed to the presence of Au^{3+} species indicating incomplete reduction of their gold oxide species under the reaction conditions used in this work (maximum reaction temperature of 674 K). The fraction of reduced gold species, expressed as $Au^0/(Au^0 + Au^{3+})$ ratio, follows the order: Au/Ce/HMS $\gg$ Au/Ce-HMS > Au/HMS (Table 3), in agreement with TPR and DRS UV–vis results. These results should be reflected in the catalytic properties during CO oxidation. By analyzing the values of the Au/Si atomic surface ratio from freshly calcined samples to used samples, we note that some increases in

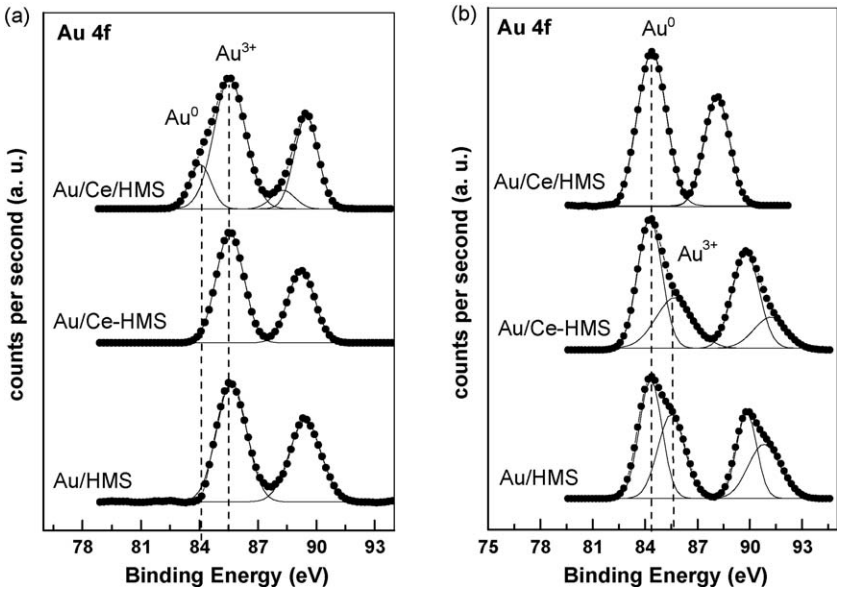

Fig. 7. XPS Au 4f core-level spectra of calcined (a) and spent Au catalysts (b).

the dispersion of gold species occurs in all samples during the reaction, under the conditions used in this work. The amount of gold species exposed on the surface of spent catalysts follows the order: Au/Ce/HMS > Au/Ce-HMS > Au/HMS. Once again, the amount of gold species exposed on the surface of Au/Ce/HMS catalyst is 22% and 88% higher than on the surfaces of Au/Ce-HMS and Au/HMS samples, respectively.

3.7. Catalytic activity

The catalytic activity of freshly calcined Au catalysts was evaluated in the CO oxidation performed in a flow-reactor at atmospheric pressure, raising reaction temperature from 293 to 673 K with a heating rate of 3 K min^{-1}. The feed mixture composition was: CO (1%), O_2 (0.5%) and N_2 (98.5%). Catalytic activity results expressed as CO conversion versus reaction temperature are shown in Fig. 8. As seen in this figure, the Au/Ce/HMS sample shows a sharp increase in CO conversion in the temperature range 293–473 K and then a period of nearly steady-state conversion was attained rapidly and maintained until a reaction temperature of 673 K. On the other hand, regarding the Au/HMS and Au/Ce-HMS catalysts, an increase of temperature from 293 to 340 K (Au/Ce-HMS) or to 460 K (Au/HMS) did not lead to an increase in CO conversion. After this initial period of operation, CO conversion over both catalysts increased sharply and then continued to increase slightly for as long as the experiment continued (673 K). Noticeably, all catalysts were active in reaction at 293 K, with the Au/Ce/HMS sample being doubly more active (ca. 35% of CO conversion) than both Au/Ce-HMS and Au/HMS samples. The ignition temperature at 50% of conversion follows the order: Au/Ce/HMS (358 K) ≫ Au/Ce-HMS (480 K) > Au/HMS (520 K). Thus, the Au/Ce/HMS catalyst clearly has a much lower ignition temperature (at 50% of conversion) compared to the other two samples. At a reaction temperature of 498 K, 100% of the CO conversion was recorded on Au/Ce/HMS sample, whereas the CO conversions for the Au/Ce-HMS and Au/HMS catalysts were 58% and 19%, respectively.

From the activity results, it can be concluded that: (i) irrespectively of the Ce incorporation method (one-pot synthesis or impregnated method), the presence of Ce ions enhances the CO oxidation ability of the Au samples; (ii) superior performance was observed when Ce ions were deposited on the HMS support by the impregnation method (Au/Ce/HMS). Comparing the performance of the Au/Ce/HMS sample with the performance of gold catalysts supported on Co_3O_5, NiO, Al_2O_3, SiO_2, CeO_2 materials [37–40], with a similar gold content to our samples and tested under similar reaction conditions to the ones used in the present work, our sample has a better performance for CO oxidation.

Finally, considering the presence of a small concentration of H_2 in the feed mixture (0.33%), one might expect the formation of H_2O

Table 3
Binding energies (eV) of core levels and surface atomic ratios of the freshly calcined and spent catalysts in the CO oxidation.

Sample	Au $4f_{7/2}$		Au/Si		$\frac{Au^0}{(Au^0+Au^{3+})}$	
	Calcined	Spent	Calcined	Spent	Calcined	Spent
Au/HMS	85.6 –	85.5 84.4	0.0024	0.0026	–	0.53
Au/Ce-HMS	85.5 –	85.5 84.4	0.0035	0.0040	–	0.65
Au/Ce/HMS	85.7 84.1	– 84.4	0.0042	0.0049	0.19	1

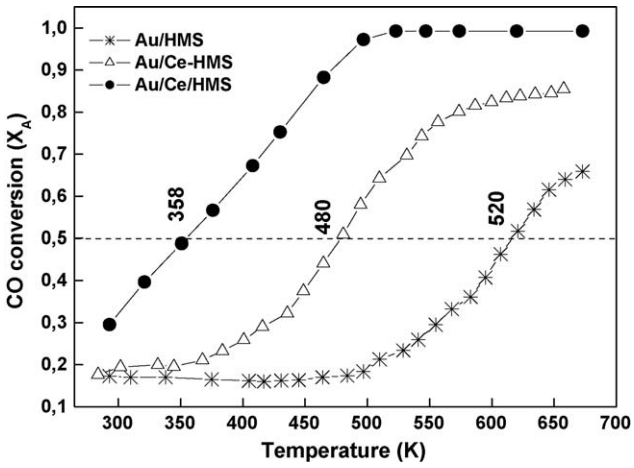

Fig. 8. Influence of reaction temperature on CO conversion in the reaction of CO oxidation over freshly calcined Au catalysts supported on HMS, Ce-HMS and Ce/HMS materials.

if CO conversion is incomplete. Indeed, traces of H_2O were detected by GC in the products of the CO oxidation reaction over all the catalysts studied, but the conversion of CO to CO_2 was almost total. The positive effect of the presence of water in the reactive feed on the catalytic activity of calcined metallic monolith coated with 1%Au/CeO_2 tested in the CO oxidation has recently been reported [41,42]. However, in our opinion, the presence of H_2O (from reactive feed or formed during the reaction) could favour the CO_2 desorption due to the hydrophobic character of the metallic Au particles.

3.8. Catalytic activity–structure correlation

In this study, all Au catalysts were prepared by the same preparation deposition–precipitation method. The catalyst characterization results clearly indicate that the textural properties of the support influenced the gold particle sizes formed during calcination at 373 K. This is because of the large differences in the migration and coalescence of the Au particles or migration of adatoms of Au (Oswald ripening) on the surface of Ce-HMS, Ce/HMS and HMS materials. Taking into account the different structural properties of the materials employed as supports, as well as the main location of the Au particles on the support surface (deduced from NS_{BET}), the highest activity of Au/Ce/HMS catalysts in the CO oxidation reaction could be explained considering the specific interaction between Au and the Ce/HMS support surface. The morphology of this support can be visualized as the presence of small domains of CeO_2 on the HMS support surface. The HRTEM results clearly indicate that Au particles are located on the HMS and not on the CeO_2. The question is whether CeO_2 modified the morphology of HMS material only and/or a synergetic effect occurs at the gold and metal oxide interface. The comparison of the Au/Si atomic ratio in Table 3 suggests that the presence of CeO_2 enhanced Au species surface exposure in the calcined and spent catalysts, with this exposure being highest in the case of Ce incorporation by impregnation of HMS material (Ce/HMS). The influence of the support morphology on the size of Au particles could be deduced from Fig. 9, which shows a linear correlation between the surface exposure of Au species in the spent catalysts (from XPS, Table 3) and their Au particle size (from HRTEM). Since gold particle size decreases with an increase in their surface exposure, it is clear that the presence of CeO_2 on the support surface favours the formation of small Au particles. Moreover, the comparison of the Au/Si atomic ratio of the fresh calcined and spent catalysts (see Table 3) indicates that, with or without Ce modification, the samples showed no sintering of Au particles during on-stream.

It is known that the absence of unpaired *d* electrons in the electronic structure of gold inhibited the chemisorption of H_2 or O_2 on its surface at ambient temperature. However, the gold can catalyse dioxygen transfer, as found, for example, in the oxidation of pentanol to pentanal by NO_2 [43]. Thus, in agreement with Deng et al. [44], we could assume that the presence of CeO_2 species on the surface of Au/Ce-HMS catalyst increases the mobility of dioxygen. This might explain the enhancement of activity on Au/Ce/HMS catalysts deduced from lowering the ignition temperature. Finally, HRTEM studies showed an interesting dependence between the gold particle sizes and ignition temperature in CO oxidation, as has been well documented by Haruta et al. [37]. Moreover, a correlation was found between the abundance of Au^0 species in the spent samples and ignition temperature (Fig. 10). Therefore, we could attribute the higher catalytic performance of the Au/Ce/HMS, under the conditions used in this work, to the best Au dispersion and presence of metallic Au^0 particles.

In short, the higher activity of the Au/Ce/HMS sample could be attributed to multiple factors such as: (i) highest dispersion of Au species on the support surface (by XPS and HRTEM), (ii) highest content of reduced metallic Au^0 particles (by DRS UV–vis and XPS), and (iii) higher redox ability of the support (higher Ce^{4+}/Ce^{3+} ratio, indicating a CeO_2 supply of oxygen in the oxidation reaction of CO) (DRS UV–vis). According to our results, we strongly believe that Ce-modified HMS material could be a suitable support for the preparation of gold catalysts for CO oxidation. Moreover, such materials could be a good candidate for the preparation of catalysts for preferential CO oxidation (PROX reaction). However, many experiments should be conducted to understand the mechanism of activation of supported gold on these systems and take advantage of the superior stability and high surface area of the HMS material.

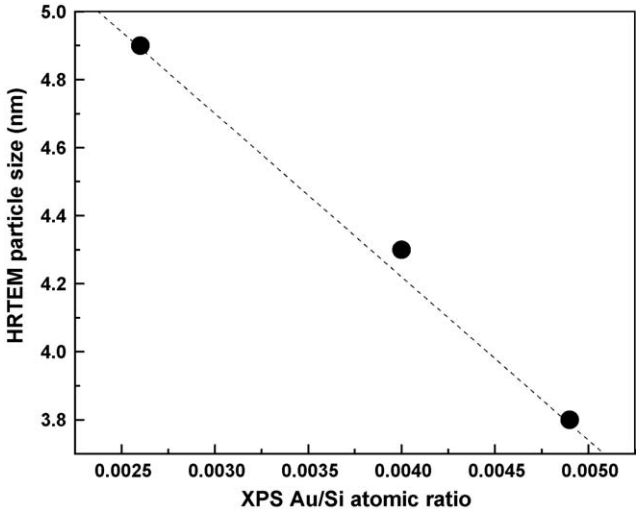

Fig. 9. Correlation between the surface exposure Au species in the spent catalysts (from XPS) and Au particle size, as determined by HRTEM of the spent catalysts.

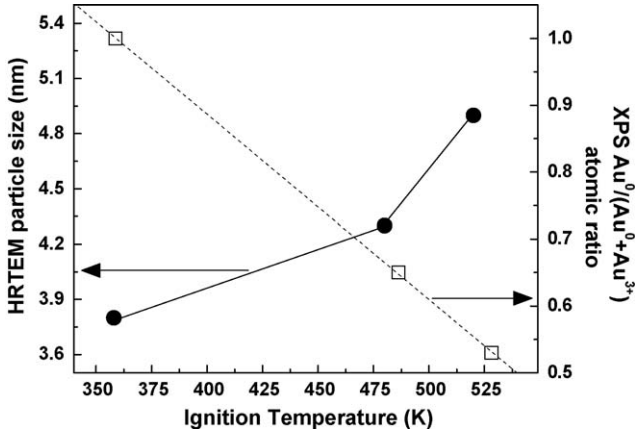

Fig. 10. Influence of the Au particle size (by HRTEM) and metallic Au^0 particles on the ignition temperature.

4. Conclusions

We have shown that the HMS material could be used successfully as a support for the preparation of gold catalysts for CO oxidation. Cerium introduction to HMS material by direct synthesis and impregnation methods (Ce-HMS and Ce/HMS, respectively) improved the catalytic performance of supported gold catalysts. A superior performance was observed when Ce ions are deposited by impregnation on the HMS support (Au/Ce/HMS), and its high performance was related to multiple factors, such as: (i) highest dispersion of Au species on the support surface (by XPS

and HRTEM), (ii) highest content of reduced metallic Au^0 particles (by DRS UV–vis and XPS), (iii) higher redox ability of the support (higher Ce^{4+}/Ce^{3+} ratio, than the supply of oxygen in the oxidation reaction of CO) and (iv) probably a synergetic effect between the gold particles and CeO_2 interface occurs, increases the catalytic performance of these sample.

Acknowledgements

T.A. Zepeda is grateful to CNyN-UNAM and UAM-I (México) for the financial support. S.A. Gómez acknowledge the financial support of Consejo Nacional de Ciencia y Tecnología (CONACyT) (Project 42292).

References

[1] J. Yang, V. Tschamber, D. Habermacher, F. Garin, P. Gilot, Appl. Catal. B: Environ. 83 (2008) 229.
[2] A.K. Neyestanaki, F. Klingstedt, T. Salmi, D.Y. Murzin, Fuel 83 (2003) 395.
[3] A.K. Datye, Q. Xu, K.C. Kharas, J.M. McCarty, Catal. Today 111 (2006) 59.
[4] G.C. Bond, D.T. Thompson, Catal. Rev. Sci. Eng. 41 (1999) 319.
[5] M. Haruta, N. Yamada, T. Kobayashi, S. Iijima, J. Catal. 115 (1989) 301.
[6] M. Haruta, S. Tsubota, T. Kobayashi, H. Kageyama, M.J. Genet, B. Delmon, J. Catal. 144 (1993) 175.
[7] M. Haruta, Cattech 6 (2002) 102.
[8] R.J.H. Grisel, B.E. Nieuwenhuys, Catal. Today 64 (2001) 69.
[9] V. Aguilar-Guerrero, B.C. Gates, Chem. Commun. (2007) 3210.
[10] O. Pozdnyakova-Tellinger, D. Teschner, A. Wootsch, J. Kröhnert, B. Steinhauer, H. Sauer, L. Toth, F.C. Jentoft, A. Knop-Gericke, Z. Paál, R. Schlögl, J. Catal. 237 (1) (2006) 17.
[11] D. Teschner, A. Wootsch, O. Pozdnyakova-Tellinger, J. Kröhnert, E. Vass, M. Hävecker, S. Zafeiratos, P. Schnörch, F.C. Jentoft, A. Knop-Gericke, R. Schlögl, J. Catal. 249 (2007) 318.
[12] M. Bandyopadhyay, O. Korsak, M.W.E. van den Berg, W. Grünert, A. Birkner, W. Li, F. Schüth, H. Gies, Micropor. Mesopor. Mater. 89 (2006) 158.
[13] M. Ruszel, B. Grzybowska, M. Łaniecki, M. Wójtowski, Catal. Commun. 8 (2007) 1284.
[14] H.P. Lin, Y.S. Chi, J.N. Lin, C.Y. Mou, B.Z. Wan, Chem. Lett. (2001) 1116.
[15] J.H. Liu, Y.Y. Chi, H.P. Lin, C.Y. Mou, B.Z. Wan, Catal. Today 93–95 (2004) 141.
[16] M.T. Bore, H.N. Pham, T.L. Ward, A.K. Datye, Chem. Commun. (2004) 1620.
[17] S.H. Overbury, L. Ortiz-Soto, H. Zhu, B. Lee, M.D. Amiridis, S. Dai, Catal. Lett. 95 (2004) 99.
[18] W. Gac, J. Gawronek, G. Wójcik, K. Kępiński, Adsorption 14 (2008) 247.
[19] T.A. Zepeda, T. Halachev, B. Pawelec, R. Nava, T. Klimova, G.A. Fuentes, J.L.G. Fierro, Chem. Mater. 17 (2005) 4062.
[20] C.T. Kresge, M.E. Leonowich, W.J. Roth, J.C. Vartuli, J.S. Beck, Nature 359 (1992) 710.
[21] A.Y. Khodakov, A. Griboval-Constant, R. Bechara, F.J. Villain, Phys. Chem. B 105 (2001) 9805.
[22] R. Mokaia, W.J. Jones, Catalysis 172 (1997) 211.
[23] S. Gotier, A. Tuel, Zeolites 15 (1995) 601.
[24] T. Chiranjeevi, P. Kumar, S.K. Maity, M.S. Rana, G. Murali Dhar, T.S.R. Prasada Rao, Micropor. Mesopor. Mater. 44 (2001) 547.
[25] T. Chiranjeevi, P. Kumar, M.S. Rana, G. Murali Dhar, T.S.R. Prasada Rao, J. Mol. Catal. 181 (2002) 109.
[26] K.B. Sundaram, P. Wahid, Phys. Rev. B 161 (1990) 163.
[27] B.M. Weckhuysen, R.A. Schoonheydt, Catal. Today 49 (1999) 441.
[28] R. Li, S. Yabe, M. Yamashita, S. Momose, S. Yoshida, S. Yin, T. Sato, Mater. Chem. Phys. 75 (2002) 39.
[29] K. Luo, T.P.S. Clair, X. Lai, D.W. Goodman, J. Phys. Chem. B 104 (2000) 3050.
[30] R. Zanella, S. Giorgio, C.-H. Shin, C.R. Henry, C. Louis, J. Catal. 222 (2) (2004) 357.
[31] G. Munteanu, L. Ilieva, R. Nedyalkova, D. Andreeva, Appl. Catal. A: Gen. 277 (2004) 31.
[32] A. Trovarelli, Catal. Rev. Sci. Eng. 38 (1999) 439.
[33] M.M. Mohammed, T.M. Salama, R.O. Ohnishi, M. Ichikawa, Langmuir 17 (2001) 5678.
[34] W.A. Pireaux, M. Leihr, P.A. Thiry, J.P. Delrue, R. Caudano, Surf. Sci. 141 (1984) 221.
[35] F. Boccuzzi, A. Chiorino, M. Manzoli, P. Lu, T. Akita, S. Ichikawa, M. Haruta, J. Catal. 202 (2001) 256.
[36] M.P. Seah, G.C. Smith, M.T. Anthony, Surf. Interface Anal. 15 (1990) 293.
[37] M. Haruta, N. Yamda, T. Kobatashi, S. Iijima, J. Catal. 115 (1989) 301.
[38] V. Idakiev, L. Ilievaa, D. Andreeva, J.L. Blin, L. Gigot, B.L. Sub, Appl. Catal. A: Gen. 243 (2003) 25.
[39] A.M. Venezia, L.F. Liotta, G. Pantaleo, V. La Parola, G. Deganello, A. Beck, Z. Koppány, K. Frey, D. Horváth, L. Guczi, Appl. Catal. A: Gen. 251 (2003) 359.
[40] S. Goluński, R. Rajaram, N. Hodge, G.J. Hutchings, C.J. Kiely, Catal. Today 72 (2002) 107.
[41] F. Romero-Sarria, A. Penkova, L.M. Martinez, M.A. Centeno, K. Hadjiivanov, J.A. Odriozola, Appl. Catal. B: Environ., in press.
[42] Y. Yang, A. Sayari, Stud. Surf. Sci. Catal. 141 (2002) 189.
[43] S.A. Nyarady, R.E. Sievers, J. Am. Chem. Soc. 107 (1985) 3726.
[44] W. Deng, J. De Jesus, H. Saltsburg, M.F. Stephanopoulos, Appl. Catal. A: Gen. 291 (2005) 126.